POLITECNICO DI TORINO
Repository ISTITUZIONALE

Interfacing Dual-Polarized Waveguide Direct Radiating Arrays with Front-End Electronics

Original
Interfacing Dual-Polarized Waveguide Direct Radiating Arrays with Front-End Electronics / Montoya-Roca, R., Vazquez-Sogorb, C., Paonessa, F., Lumia, M., Addamo, G., Peverini, O.A., Maiarelli, D., Gasparro, G., Virone, G.. - ELETTRONICO. - (2026), pp. 1-5. (20th European Conference on Antennas and Propagation (EuCAP 2026) Dublin (Ire) 19-24 April 2026) [10.23919/eucap68105.2026.11612742].

Availability:
This version is available at: 11583/3015051 since: 2026-11-17T22:17:11Z

Publisher:
IEEE

Published
DOI:10.23919/eucap68105.2026.11612742

Terms of use:

This article is made available under terms and conditions as specified in the corresponding bibliographic description in the repository

Publisher copyright
IEEE postprint/Author's Accepted Manuscript

©2026 IEEE. Personal use of this material is permitted. Permission from IEEE must be obtained for all other uses, in any current or future media, including reprinting/republishing this material for advertising or promotional purposes, creating new collecting works, for resale or lists, or reuse of any copyrighted component of this work in other works.

(Article begins on next page)

29 November 2026

Interfacing Dual-Polarized Waveguide Direct Radiating Arrays with Front-End Electronics

Roger Montoya-Roca*†, Carlos Vazquez-Sogorb *†, Fabio Paonessa†, Mauro Lumia†, Giuseppe Addamo†, Oscar A. Peverini†, Davide Maiarelli*, Giovanni Gasparro*, Giuseppe Virone†
*Thales Alenia Space, Rome, Italy, roger.montoya@thalesaleniaspace.com
†Istituto di Elettronica e di Ingegneria dell'Informazione e delle Telecomunicazioni (IEIIT)
Consiglio Nazionale delle Ricerche (CNR), Turin, Italy, roger.montoyaroca@ieiit.cnr.it

***Abstract*—This paper investigates the challenging interface between Ka-band waveguide-based arrays and the transmit/receive modules in printed circuit boards. To overcome the limitations associated with this integration, a novel and highly compact waveguide end-launcher is proposed. When combined with a waveguide polarizer, the design supports dual-circular polarization over the Ka-band downlink frequency range (17.7 – 20.7 GHz) without requiring re-meshing layers or expanders to interface with the transmit/receive modules. The proposed solution effectively addresses the constraints of conventional in-line waveguide end-launchers, which are restricted to single-mode or single-polarization excitation per port.**

***Index Terms*—Direct Radiating Arrays, Circular Polarization, Waveguide end-launcher, Phased array antennas, Multibeam antennas, Waveguide apertures, Ka-band, Microstrip to waveguide transitions, LEO SatCom, Waveguide feed element.**

I. Introduction

Direct Radiating Arrays (DRAs) have emerged as a key antenna technology for Ka-band low Earth orbit (LEO) satellite communication systems [1]. Waveguide apertures are preferred over PCB based antenna solutions owing to their inherently low losses, high power-handling capability, and superior robustness in harsh space environments [2], [3]. Furthermore, the integration of a waveguide septum polarizer enables dual-circular polarization within the waveguide section, which is crucial to prevent polarization mismatch and ensure reliable link performance [4].

DRAs are composed of hundreds of electrically small radiating elements to achieve the required gain and satisfy the EIRP specifications. The inter-element spacing is carefully selected to prevent the appearance of grating lobes within the field of view (FoV), typically up to $\pm 50^\circ$ or $\pm 60^\circ$. A triangular lattice configuration is adopted instead of a square lattice, as it allows the spacing to be increased from approximately 0.5λ to 0.6λ, providing additional space for integrating the transmit/receive (T/R) modules. However, this lattice arrangement introduces additional complexity in the RF interconnections between the front-end electronics and the radiating elements.

Each radiating element includes an independent input to apply the required amplitude and phase coefficient for beam steering. In satellite-based DRAs, the brick configuration is commonly preferred over the tile architecture, as it enables the efficient integration of thermal management pipe lines with the RF circuitry, thereby improving heat dissipation from the large number of active components. In this configuration, the RF front-ends can be mounted on vertically oriented PCBs, equally spaced according to the array's inter-element spacing, while a horizontal PCB positioned on top hosts the feeding of the waveguide radiating element.

In the cases where alignment or space constraints cannot be satisfied, a complex RF interface layer is often required to connect the input of each radiating element to the RF front-end. For this purpose, re-meshing PCB layers or waveguide expander fanouts are commonly employed [5], [6]. However, minimizing the use of such interface structures is highly desirable, as they increase insertion losses, manufacturing complexity, and overall system cost. Consequently, the optimal approach is to design a high-performance waveguide end-launcher that directly excites the fundamental modes of the waveguide, featuring two input ports positioned within the array periodicity and precisely aligned with the RF front-end PCBs. This configuration enables direct interconnection via bullet connectors, eliminating the need for extra transition layers. For such array periodicities around 9 mm, SMPM and SMPS connectors are typically employed due to their compact footprint and excellent performance at high frequencies.

In DRAs with densely packed radiating elements arranged in clustered configurations, E-probe feeding transitions oriented orthogonally to the waveguide aperture axis become impractical. Consequently, in-line feeding solutions such as coaxial to waveguide transitions [7], microstrip to waveguide transitions [8], or integrated patch antennas [9] are adopted to excite the fundamental mode at each input port of the septum polarizer within a highly compact pitch area of approximately $\lambda/4$.

This paper presents a novel and highly compact three-ridge hexagonal waveguide end-launcher capable of supporting dual-circular polarization in the Ka-band downlink frequency range (17.7 - 20.7 GHz) when combined with a waveguide polarizer that introduces a 90° phase shift between the fundamental modes [10], as illustrated in Fig. 1.

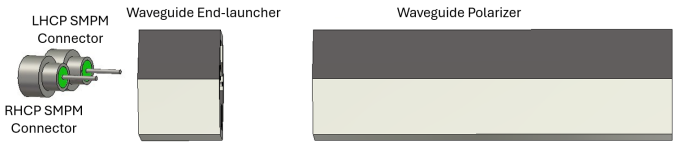


Fig. 1. Proposed Dual-Circularly polarized waveguide feed element for Ka-band DRA for LEO satellite communications.

Simulated and measured results are presented, confirming the good performance of the proposed design. The proposed design overcomes the limitations of conventional waveguide end-launchers reported in the literature, which are restricted to single-mode or single polarization excitation per port.

The paper is organized as follows. Section II discusses the proposed end-launcher configurations and their associated limitations. Section III presents the final end-launcher design and its simulated and measured performance. Finally, Section IV summarizes the main conclusions of this work.

II. End-launcher design and limitations

Septum polarizers are used as the standard solution for generating dual-circular polarized waveguide apertures. They consist of two pairs of single-mode waveguide sections separated by a thin septum within the common waveguide. This configuration supports two degenerate fundamental modes that propagate along the shared waveguide and enables the conversion of a linearly polarized input signal into either right hand circular polarization (RHCP) and left hand circular polarization (LHCP). However, this configuration restricts the end-launcher design of each waveguide section to a period smaller than $\lambda/4$, thereby limiting both the available space and the flexibility for integrating connectors within the array period.

To overcome these limitations, this paper proposes a high-performance waveguide end-launcher that employs a single common waveguide for both input ports (RHCP and LHCP), providing greater flexibility in connector placement. The proposed end-launcher is designed to excite the two fundamental modes from each input port with equal amplitude. Furthermore, a waveguide polarizer introducing a 90° phase shift between the fundamental modes is integrated after the end-launcher. Consequently, the phase difference between the fundamental modes at the end-launcher outputs must be 0° and -180° to achieve RHCP and LHCP, respectively.

A canonical waveguide section with an inter-element spacing around 0.62λ at Ka-band is below cut-off. To overcome this limitation, three ridges with 120° rotational symmetry are introduced inside the waveguide enabling propagation of the fundamental modes across the desired frequency band.

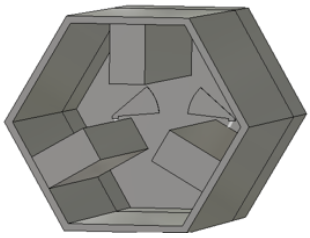
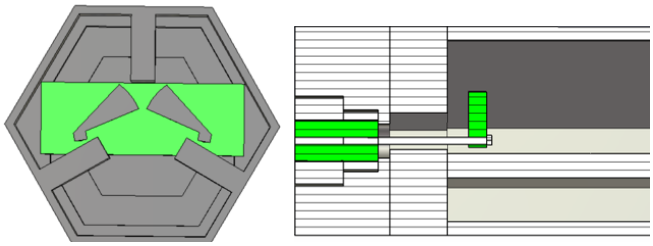


Fig. 2. Closed-ended waveguide end-launcher with $\lambda_{wg}/4$ feed position.



(a) (b)

Fig. 3. Closed-ended waveguide end-launcher with below $\lambda_{wg}/4$ feed position integrated with PCB structure. (a) Front view, (b) longitudinal view showing the integration of the Bulkhead Hermetic ST Plug connector within the waveguide wall.

The first design, illustrated in Fig. 2, employs a closed-ended waveguide end-launcher in which the excitation elements for the fundamental modes are placed at a distance of $\lambda_{wg}/4$ from the waveguide end wall to create the required back-short, thereby preventing the excitation of higher-order modes. In this configuration, the excitation elements are based on radial stub transmission lines, carefully designed to excite the fundamental modes with equal amplitude and the appropriate phase. However, in this theoretical design, the radial stubs cannot be physically supported by the waveguide or ridge structures and are fed through an idealized discrete port positioned between the ridges and the radial stubs.

Consequently, a PCB structure is introduced as a solution to support the radial stubs, as illustrated in Fig. 3. However, the PCB must be positioned inside the waveguide at a distance of $\lambda_{wg}/4$, which presents significant mechanical challenges since conventional fastening methods such as screws or adhesives cannot be used. Furthermore, the waveguide feed element cannot be manufactured as a monolithic block, as it must be divided into two parts to accommodate the PCB feeding section. To mitigate this issue, the waveguide structure is modified to include a step wide enough to support the PCB without degrading its performance. Nevertheless, an additional fixing method is still required, and this approach remains infeasible for a fully monolithic waveguide implementation. Additionally, the back-short is also achieved by reducing the waveguide period so that it operates in the evanescent mode. In this way, the PCB can be positioned closer below $\lambda_{wg}/4$ to the waveguide wall, allowing direct contact with the inner conductor of SMPM Bulkhead Hermetic ST Plug connectors.

In some applications, dual-circular polarization or polarization reconfigurability is not required, and the waveguide feed system operates in a single circular polarization. In a conventional septum polarizer, one port is connected to the active components, while the other port is terminated with a $50\ \Omega$ matched load. On the contrary, in the proposed waveguide end-launcher where both connectors share a common waveguide both connectors must still be present, even when only one fixed circular polarization is required.

Fig. 4 shows the radiation pattern performance of the closed-end waveguide end-launcher with a below $\lambda_{wg}/4$ feed position integrated into the PCB structure. The results are obtained using an ideal polarizer and a three-ridge waveguide aperture with either two or a single input feeding connector, under the infinite array approximation. The co-polar (Co-Pol) component, cross-polar (Cross-Pol) component, and cross-polar discrimination (XPD = Co-Pol - Cross-Pol) are presented at the lower, center, and upper frequencies of the operational band within the FoV.

When both input ports are present, the Co-Pol component follows a $\cos\theta_s$ distribution across the FoV, while the Cross-Pol component remains negligible, yielding a high XPD over the entire FoV. Conversely, for the configuration with only one radial stub and a single input feeding port, the Co-Pol component remains practically unchanged, whereas the Cross-Pol component increases significantly approaching 0 dB. This behavior occurs because, for example, when LHCP is excited, part of the signal reflected at the antenna aperture propagates back toward the port and is interpreted as RHCP. This reflection increases the cross-polarization level, thereby reducing the XPD to around 0 dB. Consequently, both input ports are essential in the septum polarizer and in the proposed waveguide feed element design.

III. Final Design

The previous designs were found to be infeasible due to mechanical constraints. Therefore, the proposed solution, shown in Fig. 5 in a 7-element cluster array end-launcher, consist of an open-ended waveguide end-launcher positioned above a PCB feeding layer. The waveguide is extended through the PCB using via fences. In this configuration, the $\lambda_{wg}/4$ back-short is realized by setting the PCB thickness approximately equal to $\lambda_{wg}/4$ at the center frequency of the operating band. This approach simplifies the overall structure, requiring only a few screws for the assembly.

The radial stubs are strategically positioned around $45°$ with respect to the electric fields of the two fundamental modes to couple both orthogonal modes with same amplitude and maintaining an opposite phase difference between them. The same idea in the position of the probes is proposed in [11] where an OMT featuring the -3 dB of coupling region with the two-probes at $45°$.

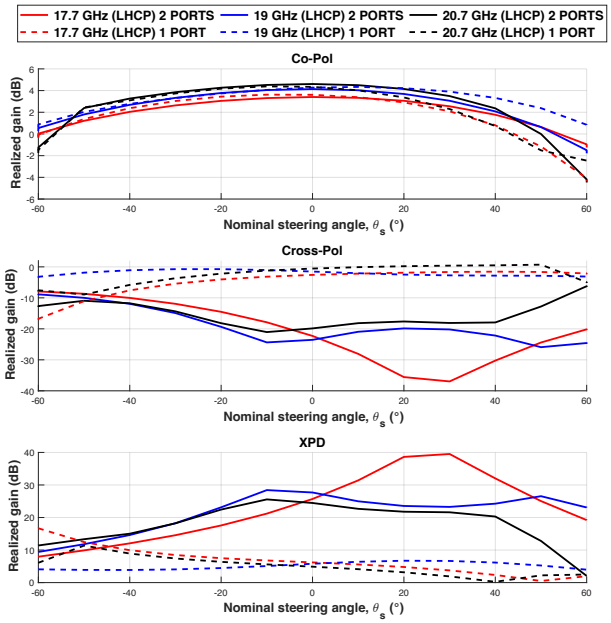
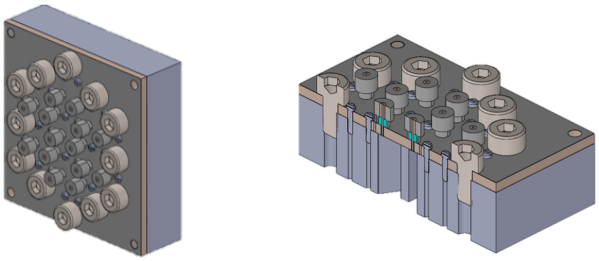


Fig. 4. Radiation pattern comparison of the closed-ended waveguide end-launcher with a below $\lambda_{wg}/4$ feed position integrated with PCB structure with two or one input feeding ports.



(a) Rear view (b) Longitudinal view

Fig. 5. (a) Rear view of the proposed waveguide end-launcher, (b) longitudinal view of the proposed waveguide end-launcher.

A 7-element cluster array end-launcher prototype is manufactured using Electrical Discharge Machining (EDM), as shown in Fig. 5. M1 screws are used to ensure reliable metal-to-metal contact between the top PCB layer and the metallic waveguide block containing the end-launcher section. M3 screws surrounding the seven elements provide a rigid mechanical and electrical joint between the PCB and the waveguide block, and they are also used to assemble the remaining feed element components and the ridged waveguide aperture. In addition, four alignment pins are placed at the corners of the array to guarantee accurate positioning. EDM is selected over other manufacturing techniques to achieve the lowest fabrication tolerances. In this case, a maximum dimensional tolerance of 10 µm is achieved. For the PCB, a maximum dimensional and position tolerance of 20 µm is provided. With these tolerances, it is verified that the performance is not significantly affected.

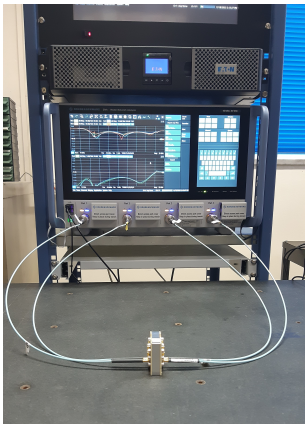


Fig. 6. Back-to-back measurement setup configuration

The performance of the end-launcher is evaluated using a back-to-back (B2B) configuration, as shown in Fig. 6.

The simulation and measurement results of the reflection and isolation coefficients for port 1 (right-hand-side port of the central element) are shown in Fig. 7. Both ports of each element exhibit the same performance. Therefore, only one port is shown for brevity. The blue solid trace represents the simulated reflection coefficient of the end-launcher with a waveguide port at the output of the waveguide section. Two resonance frequencies are identified at 18 GHz and 20 GHz, with reflection coefficients better than -24 dB within the operational band. The dashed blue line corresponds to the simulation of the end-launcher in a B2B configuration, showing an increase of approximately 4 dB at 19 GHz. The dotted blue trace represents the measured reflection coefficient, which increases to about -14 dB. This discrepancy is attributed to the fact that the simulation assumes an ideal 50 Ω connector, without accounting for the return loss of the actual connector used, which is 17 dB at 19 GHz.

Additionally, the red solid trace represents the simulated isolation coefficient of the central element, which remains below -23 dB. The dashed red trace corresponds to the simulated isolation coefficient in the B2B configuration, showing a 6 dB increase. The dotted red trace shows the measured isolation coefficient, which demonstrates excellent agreement with the simulations.

The magnitude of the transmission coefficient is shown in Fig. 8. The blue solid and dashed blue traces represent the simulated transmission coefficients of the fundamental modes from port 1. Both modes exhibit a transmission coefficient of approximately -3.18 dB, close to the desired -3 dB. The 0.18 dB difference is attributed to the end-launcher losses, considering only the dielectric losses. The solid red trace shows the simulation of the transmission coefficient in a B2B configuration from port 1, yielding a flat response with an insertion loss of 0.37 dB. As mentioned previously, the connector losses are not included in this simulation.

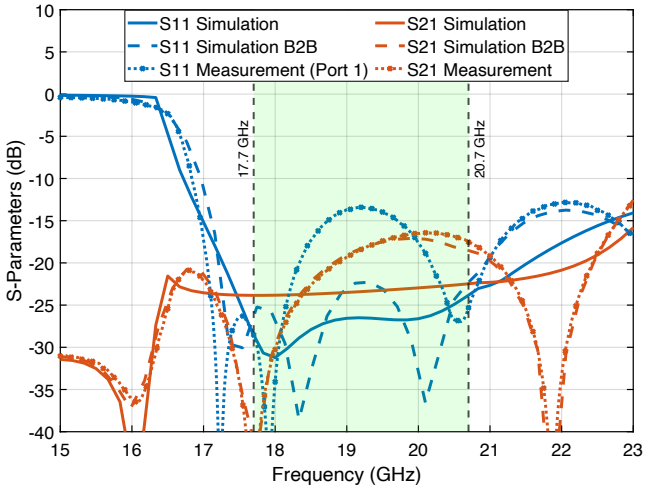


Fig. 7. Measured and simulated reflection (S_{11}) and isolation (S_{21}) coefficients at port 1 of the central element. The green box indicates the operational frequency band.

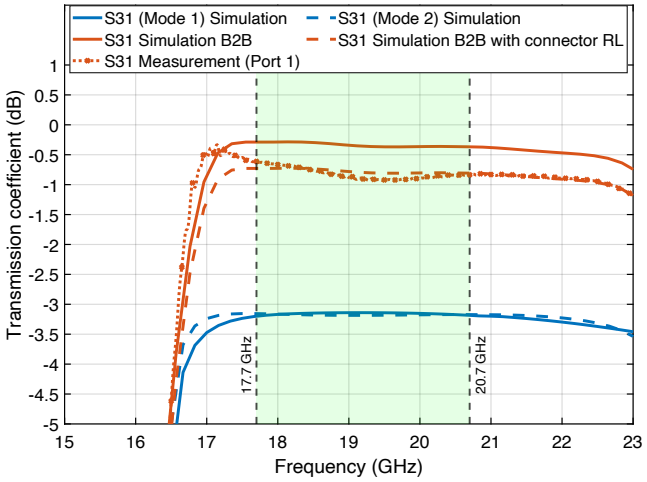


Fig. 8. Measured and simulated transmission coefficient (S_{31}) from port 1.

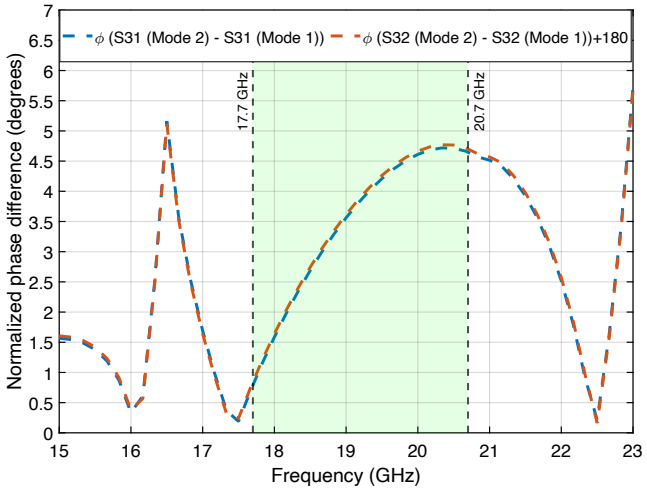


Fig. 9. Simulated phase difference between the two fundamental modes normalized to phase reference 0° and -180° for port 1 and port 2, respectively.

Therefore, the dashed red trace represents the simulation including 0.22 dB of insertion loss for each connector. This result in a total insertion loss of 0.8 dB, which shows excellent agreement with the measurement, indicated by the dotted red trace. Consequently, the insertion loss of the end-launcher alone is approximately 0.18 dB, consistent with the 0.18 dB deviation from -3 dB observed in the simulated transmission coefficients of both fundamental modes.

In Fig. 9 is shown the simulated phase difference between the fundamental modes excited in each port. Within the operating band, a phase difference of approximately 0° and -180° is achieved for port 1 and port 2, respectively. The phase difference error of the fundamental modes excited, with respect to the desired 0° and -180°, remains within 4.75°.

IV. Conclusion

This paper addresses the challenges of integrating Ka-band waveguide-based arrays with small inter-element spacing into printed circuit boards that host the active components. As a solution, a novel and highly compact dual-circularly polarized waveguide end-launcher is proposed, featuring a common waveguide shared by both RHCP and LHCP inputs, thereby increasing the flexibility in connector placement. Furthermore, the proposed end-launcher enables, for the first time in the literature, dual-linear polarization excitation at each input port, while maintaining excellent performance across the operational frequency band (17.7 – 20.7 GHz).

Initial measurements of the end-launcher in a B2B configuration are presented to assess its performance. Excellent agreement between simulations and measurements are observed for the isolation and transmission coefficient. A discrepancy is noted for the reflection coefficient, which is attributed to the simulation not accounting for the return loss of the connector.

A complete dual-circular-polarized waveguide feed element, comprising the proposed end-launcher and a waveguide polarizer, will be presented at the conference. In addition, measurement results of a 7-element cluster waveguide feed element demonstrator will be shown to accurately evaluate the performance of the end-launcher and polarizer components, with particular focus on key metrics such as cross-polarization, which quantifies the purity of the circular polarization.

Acknowledgment

Funded by the European Union, under ANTERRA 101072363 HORIZON-MSCA-2021-DN-01. Views and opinions expressed are however those of the author(s) only and do not necessarily reflect those of the European Union. Neither the European Union nor the granting authority can be held responsible for them.

References

[1] T. Chaloun et al., "Electronically Steerable Antennas for Future Heterogeneous Communication Networks: Review and Perspectives," in *IEEE Journal of Microwaves*, vol. 2, no. 4, pp. 545-581, Oct. 2022, doi: 10.1109/JMW.2022.3202626.

[2] Vazquez-Sogorb, C.; Montoya-Roca, R.; Addamo, G.; Peverini, O.A.; Virone, G. Ridged Apertures for LEO Direct Radiating Arrays in Ka-Band. *Appl. Sci*. 2024, 14, 7825. https://doi.org/10.3390/app14177825.

[3] S. Harms et al., "Waveguide Antenna Array Element with Minimized Power Amplifier Load Pull for LEO NTNs," *2024 54th European Microwave Conference (EuMC)*, Paris, France, 2024, pp. 272-275, doi: 10.23919/EuMC61614.2024.10732698.

[4] N. J. G. Fonseca and J. -C. Angevain, "C-Band Septum Polarizers With Polynomial Profile and Accurate Axial Ratio Characterization in Back-to-Back Configuration," *in IEEE Journal of Microwaves*, vol. 2, no. 4, pp. 678-689, Oct. 2022, doi: 10.1109/JMW.2022.3191440.

[5] L. Berretti et al., "Ridged Meandered Waveguides for 3-D Routing and Phase Delay Control and Its Application to Discrete Lenses," in *IEEE Transactions on Antennas and Propagation*, vol. 71, no. 5, pp. 4017-4027, May 2023, doi: 10.1109/TAP.2023.3255515.

[6] E. Menargues, M. García-Vigueras, S. Capdevila, P. Angeletti and G. Toso, "Meandered Waveguides for Active Antennas," *2021 15th European Conference on Antennas and Propagation (EuCAP)*, Dusseldorf, Germany, 2021, pp. 1-5, doi: 10.23919/EuCAP51087.2021.9411125.

[7] Simone, M.; Fanti, A.; Lodi, M.B.; Pisanu, T.; Mazzarella, G. An In-Line Coaxial-to-Waveguide Transition for Q-Band Single-Feed-Per-Beam Antenna Systems. *Appl. Sci*. 2021, 11, 2524. https://doi.org/10.3390/app11062524.

[8] L. Wen, Z. Yu, C. Chen, L. Zhu, J. Zhou and W. Hong, "Design of Evanescent Quad-Ridge Antenna With Compact Transition for 5G Millimeter-Wave Phased-Array Applications," in *IEEE Antennas and Wireless Propagation Letters*, vol. 22, no. 10, pp. 2532-2536, Oct. 2023, doi: 10.1109/LAWP.2023.3294585.

[9] M. Simeoni, C. I. Coman and I. E. Lager, "Patch end Launchers-a family of compact colinear coaxial-to-rectangular waveguide transitions," in *IEEE Transactions on Microwave Theory and Techniques*, vol. 54, no. 4, pp. 1503-1511, June 2006, doi: 10.1109/TMTT.2006.871923.

[10] H. Song, L. Jia, J. Tan, Y. Zhang and S. Liu, "Design of Wideband Quad-Ridge Waveguide Polarizer," *2023 4th China International SAR Symposium (CISS)*, Xian, China, 2023, pp. 1-6, doi: 10.1109/CISS60136.2023.10379971.

[11] N. J. G. Fonseca, "Two-Probe Waveguide Orthomode Transducer With Twofold Rotational Symmetry," in *IEEE Transactions on Microwave Theory and Techniques*, vol. 69, no. 7, pp. 3228-3235, July 2021, doi: 10.1109/TMTT.2021.3075957.